Journal of
Materials Chemistry B

COMMUNICATION

View Article Online
View Journal | View Issue

A hematite-based photoelectrochemical platform for visible light-induced biosensing†

Gyeong Min Ryu, Minah Lee, Da Som Choi and Chan Beum Park*

Cite this: *J. Mater. Chem. B*, 2015, 3, 4483

Received 15th March 2015,
Accepted 5th May 2015

DOI: 10.1039/c5tb00478k

www.rsc.org/MaterialsB

We report the first hematite-based photoelectrochemical (PEC) biosensor platform to detect NADH under visible-light irradiation. To enhance the electrical signal of photoanodes, we employed mussel-inspired polydopamine which immobilizes redox mediators on hematite. The enzymatic PEC biosensor enabled the detection of glucose, ethanol, and lactate, and even showed successful detection of glucose in human plasma, suggesting the practical usefulness of our platform.

Photoelectrochemical (PEC) detection is an attractive biosensing strategy because it inherits the benefits of electrochemical (EC) sensors, such as low cost, simple instrumentation and high sensitivity.[1] Furthermore, PEC sensing can reduce undesired background noise and enhance sensitivity by using two separate forms of signals: light (for excitation) and electricity (for detection).[2–5] In PEC cells, electrons and holes are generated by photo-excitation, which are then injected into a photocathode and a photoanode for water reduction and oxidation, respectively. Hematite (α-Fe_2O_3) is a promising photoanode material because of its strong absorption of visible light ($E_g \sim 2.1$ eV), high stability, low price, and environmentally benign characteristics.[6] While most previous studies on hematite have focused on utilizing it for solar synthesis of chemical fuels through water-splitting,[6,7] hematite has not been applied yet for biosensing despite its potential.

Here, we report on the development of novel hematite-based PEC biosensing platforms that employ NAD-dependent dehydrogenases as a biorecognition component, as illustrated in Scheme 1. NAD-dependent dehydrogenases enable a wide range of applications in enzymatic sensors[8–10] due to their catalytic capability to oxidize various analytes (*e.g.*, glucose, lactate, and alcohols). They critically require an NAD^+/NADH cofactor-couple as a redox counterpart to sustain the catalytic cycle.[11] Since direct electrochemical oxidation of NADH at 0.56 V (*vs.* SCE) induces the interference of other oxidizable analytes at the electrode, the utilization of redox mediators to enhance electron transfer rate has been considered as an attractive option for reducing the overpotential of NADH oxidation.[12–14] A sensitive and practical platform for EC and PEC biosensors requires stable immobilization and retention of mediators on the electrode surface.[15,16] In the current work, we have employed polydopamine (PDA) coating as a simple way to immobilize redox mediators on the photoelectrode. PDA, a mimic of adhesive proteins in mussels, enables one-step functionalization of any type of material surface,[17,18] and allows facile immobilization of organic dyes, providing suitable environments to facilitate catalytic reactions.[19] Using the PDA coating, we combined Nile Blue (NB), a redox mediator for electrocatalytic NADH oxidation,[20,21] with hematite, a visible-light active photo-electrode, to facilitate efficient electron transfer from NADH to the photoanode. As illustrated in Scheme 1, NB facilitates

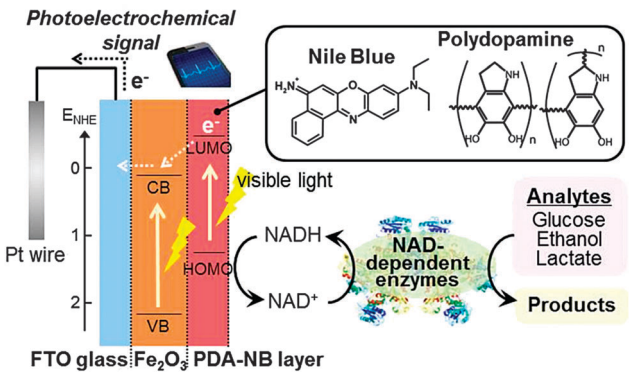

Scheme 1 Schematic illustration of the PEC biosensor platform based on the PDA–NB/Fe_2O_3 photoanode, which is used to detect NADH and various substrates by employing NAD-dependent enzymes such as glucose dehydrogenase (GDH), alcohol dehydrogenase (ADH), and lactate dehydrogenase (LDH). A redox mediator for NADH oxidation, NB, is successfully immobilized on hematite film *via* PDA coating. Photocatalytic NADH oxidation by NB generates an electrical signal that is proportional to the concentration of NADH and amplified by photo-excited electrons from a hematite-based photoanode.

Department of Materials Science and Engineering, Korea Advanced Institute of Science and Technology (KAIST), 335 Science Road, Yuseong-gu, Daejeon 305-701, Republic of Korea. E-mail: parkcb@kaist.ac.kr; Fax: +82 42-350-3310; Tel: +82 42-350-3340

† Electronic supplementary information (ESI) available. See DOI: 10.1039/c5tb00478k

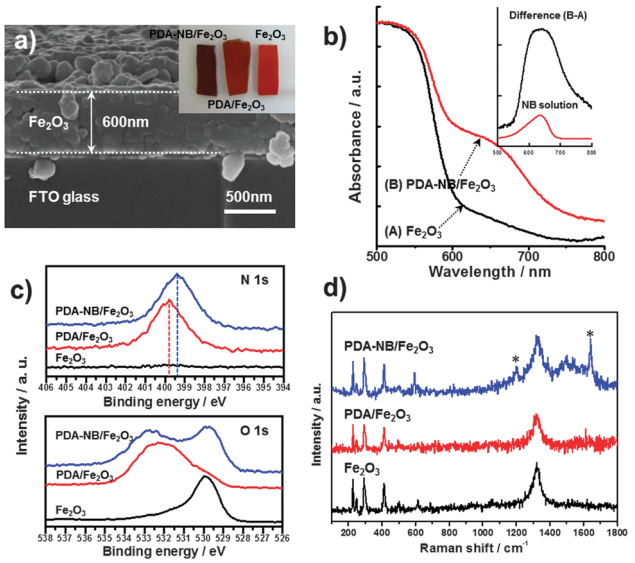

Fig. 1 Characterization of the PDA–NB coating layer on hematite. (a) SEM image of cross-section view showing the thickness of hematite film. Inset photograph shows color change of the hematite photoanode before and after coating. (b) Absorbance spectra of (A) hematite and (B) PDA–NB-coated hematite (PDA–NB/Fe_2O_3), showing significant increase of absorbance in 600–700 nm, which corresponds to the absorption peak of NB solution (inset). (c) XPS spectra for N1s and O1s peaks. (d) Raman spectra of hematite, PDA-coated hematite (PDA/Fe_2O_3) and PDA–NB/Fe_2O_3. Peaks expected from NB are indicated by asterisks.

selective oxidation of NADH and the visible-light illumination induces electron transfer from NB to hematite. As a result, the photoexcited electron transfer amplifies the electrical signal from the oxidation of analytes by NAD-dependent dehydrogenases.

We synthesized hematite film through two-step annealing at 550 °C and 800 °C on an FTO glass substrate. The X-ray diffraction (XRD) pattern of the pristine hematite film is shown in Fig. S1a (ESI†). The peaks marked with red circles clearly indicate a single crystal of α-Fe_2O_3 (JCPDS, PDF-#33-0664) without any trace of impurities. The synthesized bare Fe_2O_3 exhibited a worm-like structure and retained the same morphology after the PDA coating (Fig. S1b, ESI†). The cross-sectional scanning electron microscopic (SEM) image of a bare hematite film is presented in Fig. 1a, which shows that the film thickness is approximately 600 nm.

To fabricate PDA–NB-coated hematite film (PDA–NB/Fe_2O_3), we immersed as-synthesized hematite film in a mixed solution of dopamine and NB for 2 hours and washed it with deionized water for 14 hours. According to the change in UV-vis absorbance, approximately 68.7% of NB remained in the PDA layer after 14 hours of washing, which is attributed to π–π interaction between aromatic rings in PDA and NB forming a stable PDA–NB hybrid coating layer. After coating the hematite with either PDA or PDA–NB, the film color changed from bright orange-red to dark red (Fig. 1a, inset). Fig. 1b shows strong absorption of bare hematite in the visible light range below 600 nm, which corresponds to the band gap energy (~2.1 eV) of hematite. The PDA–NB coating induced a significant shift in light absorption of hematite film to the range of 600–700 nm due to characteristic absorption of NB, while PDA-coated hematite (PDA/Fe_2O_3) exhibited only a slight change. To further confirm the presence of NB on the surface of Fe_2O_3, we analyzed the surface elements by X-ray photoelectron spectroscopy (XPS) (Fig. 1c and Fig. S4a, ESI†). A distinguishable N1s peak was observed at the binding energy of 399.8 eV and 399.4 eV for PDA/Fe_2O_3 and PDA–NB/Fe_2O_3, respectively, which originated from nitrogen atoms in PDA and NB. The surface coating of hematite with PDA and NB also affected the shape of the O1s peak. While bare hematite showed the lattice oxygen in Fe_2O_3 centered at 530.1 eV,[22] two other spectra exhibited wide and asymmetric peaks at higher binding energies, indicating that the coating with PDA and NB changes the surface properties of hematite. Also, Raman spectroscopic analysis evidently supported the presence of NB; the Raman spectrum of PDA–NB/Fe_2O_3 in Fig. 1d shows distinctive peaks at 1640 and 1200 cm^{-1} that correspond to NB (Fig. S4b, ESI†), while two other Raman spectra of samples without NB exhibit no signal.

To investigate the activity of NB in the PDA layer for NADH oxidation, we examined PEC behaviors of hematite-based photoelectrodes using linear sweep voltammetry in a phosphate buffer (50 mM, pH 7.5). As shown in Fig. 2a and b, the photocurrents from both PDA/Fe_2O_3 and PDA–NB/Fe_2O_3 photoelectrodes began to increase upon visible-light irradiation at over 0.1 V, while negligible current was observed under dark conditions (data not shown). These anodic currents resulted from photocatalytic water splitting by photo-generated electrons and holes in the hematite photoanodes. The addition of NADH (1 mM) induced twice the oxidation current at 0.3 V in the PDA–NB/Fe_2O_3 photoelectrode upon visible-light illumination, which is attributed to the oxidation of both water and NADH, while the PDA/Fe_2O_3 photoelectrode exhibited only a slight increase of photocurrent. We also

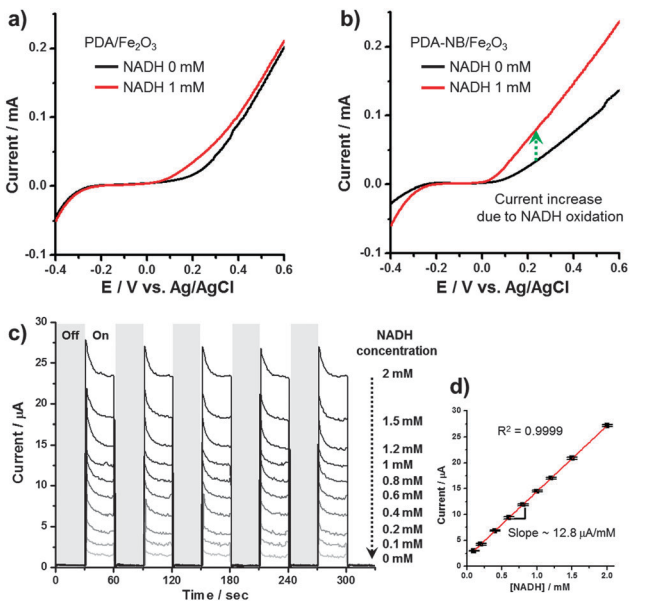

Fig. 2 Current–potential characteristics of (a) PDA/Fe_2O_3 and (b) PDA–NB/Fe_2O_3 with and without 1 mM NADH under visible light. (c) Photocurrent response and (d) calibration plot of PDA–NB/Fe_2O_3 photoanode at various NADH concentrations. As the NADH concentration increases, the photocurrent increases linearly with a correlation coefficient of 0.9999.

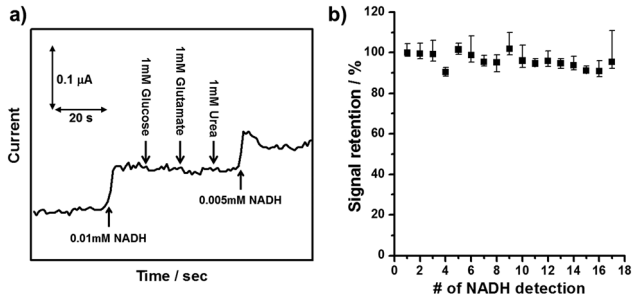

Fig. 3 (a) Photocurrent response of the PDA–NB/Fe_2O_3 photoanode in 50 mM phosphate buffer (pH 7.5) with successive addition of NADH (0.01 mM and 0.005 mM) and interference molecules (glucose, glutamate, and urea) at a concentration of 1 mM. (b) Stability test of the PDA–NB/Fe_2O_3 photoanode for NADH oxidation by measuring photocurrent repetitively. Points and error bars represent the average of photocurrent signals and the maximum and minimum values of each measurement.

conducted electrochemical impedance spectroscopy measurements to further confirm the catalytic effect of NB in the PDA layer for NADH oxidation (Fig. S5, ESI†). The Nyquist plots for bare PDA and NB-incorporated PDA films show that NB incorporation clearly decreases the charge transfer resistance in the NADH solution under visible light illumination. This result indicates that NB molecules incorporated in the PDA layer work effectively as a redox mediator for NADH oxidation, facilitating electron transfer between the electrode and the solution.

Since applied potential may affect photocurrent response in the trade-off between the elimination of possible interferences and the intensification of the sensing signal, we investigated the photo-response of PDA–NB/Fe_2O_3 electrodes under different applied potentials (Fig. S6, ESI†). While anodic photocurrent increased gradually in the range of applied potential from −0.15 V to 0 V, its rate of increase became drastic above 0 V. The current increase between 0 V and 0.05 V was four times greater than that between −0.05 V and 0 V. Accordingly, we selected 0.05 V as an applied potential for further PEC measurements. Fig. 2c presents the photocurrent profiles of the PDA–NB/Fe_2O_3 photoanode with NADH solution at different concentrations (0 to 2 mM). The photocurrent was linearly correlated to the NADH concentration with the equation I (μA) = 12.76C (mM) + 1.702 (Fig. 2d). The limit of detection (LOD) of the PDA–NB/Fe_2O_3 photoanode for NADH was approximately 4.65 μM. The sensitivity was evaluated to be approximately 12.8 μA mM^{-1}, which is much better than previous reports on PEC biosensors.[23,24] In contrast, the PDA/Fe_2O_3 photoanode (that is, without NB) exhibited poor performance in NADH detection (LOD: 89.8 μM, sensitivity: 1.52 μA mM^{-1}) (Fig. S7, ESI†), which indicates that inefficient electron transfer occurs on the electrode surface in the absence of NB, slowing down electron transport and hindering signal detection. In the PDA/Fe_2O_3 photoanode, we speculate that only holes generated internally by photo-excitation of hematite can oxidize NADH, resulting in the loss of NB effect on NADH oxidation and a low electrical signal.[25,26]

We investigated the selectivity of the PDA–NB/Fe_2O_3-based PEC sensor for NADH detection by employing glucose, glutamate, and urea as interfering substances under visible-light irradiation (Fig. 3a). We observed an immediate amperometric signal upon injection of NADH solution (0.01 mM), but negligible response was detected after a successive addition of interfering chemicals (1 mM each). We could detect an even lower concentration of NADH (0.005 mM) after adding other chemicals. This result indicates that our PDA–NB/Fe_2O_3-based PEC sensor has a reasonable selectivity towards NADH detection over other possible analytes in NAD-dependent enzymatic biosensing. We further tested the reproducibility of the PDA–NB/Fe_2O_3-based PEC sensor by measuring electrical signals from an NADH solution (0.2 mM) repeatedly. Fig. 3b shows the average values of photocurrent for each measurement with error bars, where the relative standard deviation was 3.69% and the response of the PEC NADH sensor remained at 95.5% of the initial response after 10 weeks. This result indicates that the PDA–NB/Fe_2O_3-based PEC sensor is stable for at least over 2 months, giving reliable signals in repetitive detection.

To demonstrate the utility of the PDA–NB/Fe_2O_3-based PEC platform as a versatile enzymatic biosensor, we applied the platform for the detection of glucose, ethanol, and lactate, using glucose dehydrogenase (GDH), alcohol dehydrogenase (ADH), and lactate dehydrogenase (LDH). These enzymes can catalyze the oxidation of their substrates when coupled with the reduction of NAD^+. Upon irradiation with visible light, the PDA–NB/Fe_2O_3 photoanode exhibited an immediate response of photocurrent to the oxidation of glucose at different concentrations (0–2 mM) in a phosphate buffer (pH 7.5) containing 10 mM NAD^+ (Fig. 4a). The LOD of glucose was found to be

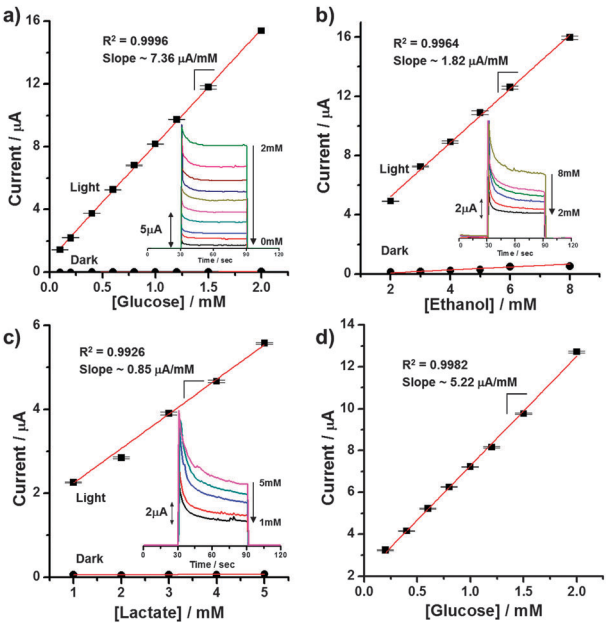

Fig. 4 Photoelectrochemical sensing of various substrates with NAD-dependent dehydrogenases. Calibration plot for (a) glucose, (b) ethanol, and (c) lactate of the PDA–NB/Fe_2O_3 photoanode under light and dark conditions. Applied potential 0.05 V *vs.* Ag/AgCl in 50 mM phosphate buffer (pH 7.5) containing 10 mM NAD^+ and 200 U of glucose dehydrogenase (GDH) or 200 U of alcohol dehydrogenase (ADH). Insets are photocurrent response at various substrate concentrations. (d) Calibration plot for glucose in a diluted human plasma solution, showing a linear relationship with glucose concentration.

approximately 25.2 μM with a sensitivity of 7.36 μA mM^{-1}. Also, the PEC detection of ethanol and lactate at different concentrations resulted in LODs of 151 μM and 471 μM, and sensitivities of 1.82 μA mM^{-1} and 0.85 μA mM^{-1}, respectively (Fig. 4b and c). We further performed PDA–NB/Fe_2O_3-based PEC sensing in human plasma solutions with glucose dissolved at different concentrations (Fig. 4d). Our analysis showed a reasonable LOD (59.4 μM) and sensitivity (5.22 μA mM^{-1}), indicating that the hematite-based PEC sensor is viable for practical applications.

Conclusions

The first hematite-based PEC biosensor platform is developed and applied for the detection of NADH under visible-light irradiation. Unlike TiO_2-based PEC sensors, hematite can absorb a wide range of visible light because of its narrow band gap energy. A simple dip-coating of hematite in PDA solution enabled stable immobilization of a redox mediator (*i.e.*, NB) on the hematite surface. The PEC measurements verified that NB incorporated in the PDA layer has a catalytic effect on NADH oxidation and facilitates electron transfer. The PDA–NB-coated hematite film exhibited sensitive NADH detection with a limit of 4.65 μM and a sensitivity of 12.8 μA mM^{-1}, along with good selectivity, stability, and reproducibility. Glucose sensing in human plasma resulted in reasonable LOD and sensitivity, demonstrating practical usefulness of the PDA–NB/Fe_2O_3-based PEC biosensor. The utilization of a single cofactor-couple (NAD^+/NADH) in numerous NAD-dependent enzymes enabled versatile detection of many relevant substrates, such as glucose, ethanol, and lactate. A simple and generic hematite-based biosensor platform will be useful in the future development of visible-light-driven PEC biosensors.

Acknowledgements

This study was supported by grants from the National Research Foundation (NRF) *via* the National Leading Research Laboratory (NRF-2013R1A2A1A05005468) and the Intelligent Synthetic Biology Center of Global Frontier R&D Project (2011-0031957), Republic of Korea.

Notes and references

1 J. Tang, Y. Wang, J. Li, P. Da, J. Geng and G. Zheng, *J. Mater. Chem. A*, 2014, **2**, 6153–6157.
2 W.-W. Zhao, J.-J. Xu and H.-Y. Chen, *Chem. Soc. Rev.*, 2014, 729–741.
3 Y. Dilgin, L. Gorton and G. Nisli, *Electroanalysis*, 2007, **19**, 286–293.
4 H. B. Yildiz, R. Freeman, R. Gill and I. Willner, *Anal. Chem.*, 2008, **80**, 2811–2816.
5 K. Wang, J. Wu, Q. Liu, Y. Jin, J. Yan and J. Cai, *Anal. Chim. Acta*, 2012, **745**, 131–136.
6 K. Sivula, F. Le Formal and M. Grätzel, *ChemSusChem*, 2011, **4**, 432–449.
7 P. S. Bassi, Gurudayal, L. H. Wong and J. Barber, *Phys. Chem. Chem. Phys.*, 2014, **16**, 11834–11842.
8 R. Freeman, R. Gill, I. Shweky, M. Kotler, U. Banin and I. Willner, *Angew. Chem., Int. Ed.*, 2009, **48**, 309–313.
9 H. Teymourian, A. Salimi and R. Hallaj, *Biosens. Bioelectron.*, 2012, **33**, 60–68.
10 B. Reuillard, A. Le Goff and S. Cosnier, *Chem. Commun.*, 2014, **50**, 11731–11734.
11 F. Hollmann, I. W. C. E. Arends and K. Buehler, *ChemCatChem*, 2010, **2**, 762–782.
12 A. Radoi and D. Compagnone, *Bioelectrochemistry*, 2009, **76**, 126–134.
13 E. Al-Jawadi, S. Pöller, R. Haddad and W. Schuhmann, *Microchim. Acta*, 2012, **177**, 405–410.
14 P.-P. Gai, C.-E. Zhao, Y. Wang, E. S. Abdel-Halim, J.-R. Zhang and J.-J. Zhu, *Biosens. Bioelectron.*, 2014, **62**, 170–176.
15 S. Kochius, A. Magnusson, F. Hollmann, J. Schrader and D. Holtmann, *Appl. Microbiol. Biotechnol.*, 2012, **93**, 2251–2264.
16 M. Moyo, J. O. Okonkwo and N. M. Agyei, *Sensors*, 2012, **12**, 923–953.
17 Y. B. Lee, Y. M. Shin, J.-h. Lee, I. Jun, J. K. Kang, J.-C. Park and H. Shin, *Biomaterials*, 2012, **33**, 8343–8352.
18 S. M. Kang, N. S. Hwang, J. Yeom, S. Y. Park, P. B. Messersmith, I. S. Choi, R. Langer, D. G. Anderson and H. Lee, *Adv. Funct. Mater.*, 2012, **22**, 2949–2955.
19 M. Lee, J. U. Kim, J. S. Lee, B. I. Lee, J. Shin and C. B. Park, *Adv. Mater.*, 2014, **26**, 4463–4468.
20 C. X. Cai and K. H. Xue, *Anal. Chim. Acta*, 1997, **343**, 69–77.
21 F. S. Saleh, M. R. Rahman, F. Kitamura, T. Okajima, L. Mao and T. Ohsaka, *Electroanalysis*, 2011, **23**, 409–416.
22 J. Y. Kim, J.-W. Jang, D. H. Youn, G. Magesh and J. S. Lee, *Adv. Energy Mater.*, 2014, **4**, 1400476.
23 G.-L. Wang, J.-J. Xu and H.-Y. Chen, *Biosens. Bioelectron.*, 2009, **24**, 2494–2498.
24 A. K. Samantara, S. Chandra Sahu, B. Bag, B. Jena and B. K. Jena, *J. Mater. Chem. A*, 2014, **2**, 12677–12680.
25 L. Xu, J. Xia, L. Wang, J. Qian, H. Li, K. Wang, K. Sun and M. He, *Chem. – Eur. J.*, 2014, **20**, 2244–2253.
26 J. Yang, P. Gao, Y. Liu, R. Li, H. Ma, B. Du and Q. Wei, *Biosens. Bioelectron.*, 2015, **64**, 13–18.

